Prostate Cancer: Apparent Diffusion Coefficient Map with T2-weighted Images for Detection—A Multireader Study[1]

Hyun Kyung Lim, MD
Jeong Kon Kim, MD
Kyung Ah Kim, MD
Kyoung-Sik Cho, MD

Purpose: To retrospectively assess the incremental value of an apparent diffusion coefficient (ADC) map combined with T2-weighted magnetic resonance (MR) images compared with T2-weighted images alone for prostate cancer detection by using a pathologic map as the reference standard.

Materials and Methods: This retrospective study was approved by the institutional review board; informed consent was waived. The study included 52 patients (mean age, 65 years ± 5 [standard deviation]; range, 48–76 years) who underwent endorectal MR imaging and step-section histologic examination. Three readers with varying experience levels reviewed T2-weighted images alone, the ADC map alone, and T2-weighted images and ADC maps. The prostate was divided into 12 segments. The probability of prostate cancer in each segment on MR images was recorded with a five-point scale. Areas under the receiver operating characteristic curve (AUCs) were compared by using the *Z* test; sensitivity and specificity were determined with the *Z* test after adjusting for data clustering.

Results: AUC of T2-weighted and ADC data (reader 1, 0.90; reader 2, 0.88; reader 3, 0.76) was greater than that of T2-weighted images (reader 1, 0.79; reader 2, 0.75; reader 3, 0.66) for all readers ($P < .0001$ in all comparisons). AUC of T2-weighted and ADC data was greater for readers 1 and 2 than for reader 3 ($P < .001$). Sensitivity of T2-weighted and ADC data (reader 1, 88%; reader 2, 81%; and reader 3, 78%) was greater than that of T2-weighted images (reader 1, 74%; reader 2, 67%; reader 3, 67%) for all readers ($P = .01$ for reader 1; $P = .02$ for readers 2 and 3). Specificity of T2-weighted and ADC data was greater than that of T2-weighted images for reader 1 (88% vs 79%, $P = .03$) and reader 2 (89% vs 77%, $P < .001$).

Conclusion: The addition of an ADC map to T2-weighted images can improve the diagnostic performance of MR imaging in prostate cancer detection.

[1] From the Department of Radiology, Asan Medical Center, University of Ulsan, 388-1 Poongnap-dong, Songpa-gu, Seoul, 138-736, South Korea. Received January 30, 2008; revision requested March 26; revision received June 10; accepted June 28; final version accepted July 23. Supported by the Korea Research Foundation Grant funded by the Korean government (MOEHRD, Basic Research Promotion Fund) (KRF-2006-E00406) and by the Korea Science and Engineering Foundation grant funded by the Korean government (MOST) (No. R01-2006-000-10998-0). **Address correspondence to** J.K.K. (e-mail: *rialto@amc.seoul.kr*).

Although endorectal magnetic resonance (MR) imaging has been widely used for detection and localization of prostate cancer prior to treatment, this modality has been noted to be limited because of unsatisfactory sensitivity and specificity for prostate cancer detection (1–3).

Recent hardware and software improvement allows the expanded use of diffusion-weighted imaging for the differentiation of cancer tissue from noncancerous tissue, on the basis of the fact that cancer tissue generally tends to have more restricted diffusion than noncancerous tissue because of its high cell densities and abundant intra- and intercellular membranes (1). Investigators have noted that the apparent diffusion coefficient (ADC) is significantly lower in prostate cancer than in noncancerous tissue, thereby suggesting the feasibility of an ADC map for prostate cancer detection (1,3–7).

Most previous studies (7–11) on diffusion-weighted imaging of the prostate involved the comparison of the ADC of prostate cancer with that of noncancerous tissue by using regions-of-interest measurements. However, a study of the actual value of the ADC for prostate cancer detection requires a more systematized study, in which multiple readers independently interpret images and a dedicated lesion-by-lesion analysis is performed to compare MR imaging and histologic findings.

The purpose of our study was to retrospectively assess the incremental value of an ADC map combined with T2-weighted images compared with T2-weighted images alone for prostate cancer detection by using a pathologic map from radical prostatectomy as the reference standard.

Advances in Knowledge

- The area under the receiver operating characteristic curve (AUC), sensitivity, and accuracy of T2-weighted images and apparent diffusion coefficient (ADC) maps (0.76–0.90, 78%–88%, and 68%–88%, respectively) are greater than those of T2-weighted images alone, irrespective of reader experience.
- The accuracy of T2-weighted images and ADC maps depends on the level of the reader's experience, as the AUC was greater for readers with a high or intermediate level of experience (0.88–0.90) than for the reader with a low level of experience (0.76).

Materials and Methods

This retrospective study was approved by the institutional review board of Asan Medical Center for human investigation, and the requirement for informed consent was waived.

Patients

The flow diagram for patient selection is summarized in Figure 1. Our primary patient selection criteria were as follows: *(a)* patients underwent radical prostatectomy for pathologically proved prostate cancer at our institution between March 2005 and February 2007 and *(b)* patients underwent preoperative prostate MR imaging examination, which included both T2-weighted and diffusion-weighted imaging with a 1.5-T MR unit by using the combination of an endorectal coil and phased-array pelvic coils. At our institution, prostate MR imaging examination is performed with both 1.5-T and 3.0-T units, and patients are randomly assigned to either of the two units. During the same period, preoperative prostate MR imaging examinations were performed with a 1.5-T unit in 67 patients and with a 3.0-T unit in 72 patients. We suggested that endorectal T2-weighted imaging at 1.5 T is more adequate for the comparison of the accuracy of diffusion-weighted and T2-weighted imaging in prostate cancer detection because the accuracy of endorectal T2-weighted imaging with a 1.5-T unit had been more widely reported in previous studies. Therefore, this study included only patients who underwent endorectal MR imaging examination with a 1.5-T unit. According to the primary criteria, 64 patients were selected. From these patients, 12 were excluded for the following reasons: *(a)* image distortion caused by hip prostheses or patient motion was too severe for readers to interpret ($n = 5$); *(b)* patients' pathologic maps were unavailable ($n = 3$); *(c)* MR imaging was performed within 6 weeks of prostate biopsy ($n = 3$); and *(d)* hormone treatment was administered prior to MR imaging ($n = 1$).

Consequently, 52 patients (mean age, 65 years ± 5 [standard deviation]; range, 48–76 years) were included in our study. The time interval between MR imaging examination and radical prostatectomy was 11 days ± 10 (range, 2–38 days). The Gleason score of the prostate cancer was 7.4 ± 1.5 (range, 6–9). The preoperative prostate-specific antigen level ranged from 1.2 to 79.6 ng/mL (mean, 10.5 ng/mL ± 8.2). The clinical stage ranged from T2aN0M0 to T3bN1M0, with a median stage of T2cN0M0.

Implications for Patient Care

- The addition of diffusion-weighted imaging to the MR imaging protocol can improve the detection and localization of prostate cancer.
- T2-weighted images and ADC maps can be more accurately interpreted by radiologists with a high level of experience.

Published online before print
10.1148/radiol.2501080207

Radiology 2009; 250:145–151

Abbreviations:
ADC = apparent diffusion coefficient
AUC = area under the ROC curve
ROC = receiver operating characteristic

Author contributions:
Guarantors of integrity of entire study, H.K.L., J.K.K.; study concepts/study design or data acquisition or data analysis/interpretation, all authors; manuscript drafting or manuscript revision for important intellectual content, all authors; manuscript final version approval, all authors; literature research, H.K.L., J.K.K.; clinical studies, all authors; statistical analysis, H.K.L., J.K.K.; and manuscript editing, all authors

Authors stated no financial relationship to disclose.

MR Imaging Examination

All MR examinations were performed with a 1.5-T MR unit (Avanto; Siemens, Erlangen, Germany) by using the combination of an endorectal coil (Prostate Coil-BPX; Medrad, Pittsburgh, Pa) and a six-channel phased-array coil. The maximum gradient specifications were 45 mT/m for amplitude and 200 mT/m/sec for slew rate. Hyoscine butylbromide (Buscopan; Boehringer Ingelheim, Ingelheim, Germany) (20 mg) was injected intramuscularly immediately prior to beginning the MR imaging examination to reduce peristalsis.

Transverse T1-weighted images (repetition time msec/echo time msec, 400–700/10–14; section thickness, 4 mm; intersection gap, 0 mm; field of view, 22 cm; and matrix, 256 × 192) and transverse, coronal, and sagittal T2-weighted fast spin-echo images (4310–4370/80–90 [effective]; echo train length, 15; matrix, 768 × 768; section thickness, 4 mm; intersection gap, 0 mm; and field of view, 22 cm) of the prostate and seminal vesicles were obtained.

Transverse diffusion-weighted images were obtained by using a single-shot spin-echo echo-planar imaging sequence with the following parameters: 3400/117 and *b* values of 0 and 1000 sec/mm^2. Full echo information was obtained with a bandwidth of 1220 Hz/pixel and a matrix size of 256 × 256. The field of view was 22 cm, with 4-mm section thickness and no intersection gap, covering the entire prostate and seminal vesicles. The orientation and location of these images were prescribed identically to the transverse T2-weighted prostate images.

In the presence of diffusion-sensitizing gradients, the ADC was given by using the following equation: $ADC = (-1/b) \cdot \ln(S_b/S_0)$, where S_b and S_0 are the signal intensities with and without diffusion weighting, respectively, and b is the diffusion-sensitizing factor (b value). ADC maps were constructed according to this equation on the basis of a voxelwise calculation.

Histologic Examination and Image Correlation

After prostate resection, each specimen was step-sectioned into 4-mm slices, as previously described (12). As a routine pathologic examination for prostate cancer, cancer foci were outlined in ink on step-section pathologic slices of the prostate by faculty pathologists in our institution. A faculty radiologist (K.S.C., with 20 years of experience in interpreting prostate MR images) matched the step-section pathologic slices with corresponding T2-weighted images and ADC maps. Landmarks used for the alignment of MR images with histologic slices included the morphologic features of the peripheral zone, central gland, apex, and base of the prostate, as well as cysts, calcifications, the verumontanum, and the urethra, as described in a previous study (6,13).

MR Image Analysis

T2-weighted images and ADC maps for each case were interpreted by three independent readers (J.K.K., K.A.K., H.K.L.) who were unaware of clinical and histologic findings. The three readers knew that all patients in the study had biopsy-proved prostate cancer. Reader 1 (J.K.K.) was a radiologist with a high level of experience (ie, faculty radiologist in the genitourinary division who had interpreted at least 800 prostatic MR images in 12 years); reader 2 (K.A.K.) was a radiologist with an intermediate level of experience (ie, fellow radiologist in the genitourinary division who had interpreted approximately 150 prostatic MR images in 8 years); and reader 3 (H.K.L.) was a radiologist with a low level of experience (ie, 4th-year resident in the radiology department who had interpreted approximately 60 prostatic MR images in the 3 years prior to the start of this study).

To systematize the prostate image evaluation, each prostate was divided into a total of 12 segments. Each prostate was divided into three levels: the base, midgland, and apex in both the right and left lobes. In both halves at each level, the gland was then further subdivided into the transitional zone and the peripheral zone. The base was determined to be the region extending from the cranial margin of the prostate to the widest transverse diameter of the prostate. The midgland was defined as the region between the widest transverse diameter and the orifices of the ejaculatory ducts at the verumontanum. The apex was defined as the region inferior to the midgland.

All readers independently reviewed the T2-weighted images alone, the ADC map alone, and a combination of the T2-weighted images and ADC maps. The three data sets in each patient were randomly interpreted in different sessions at 4-week intervals.

The presence of cancer in the peripheral zone on T2-weighted images or ADC maps was suggested when an area of nodular low signal intensity was noted. In the central gland, the

Figure 1

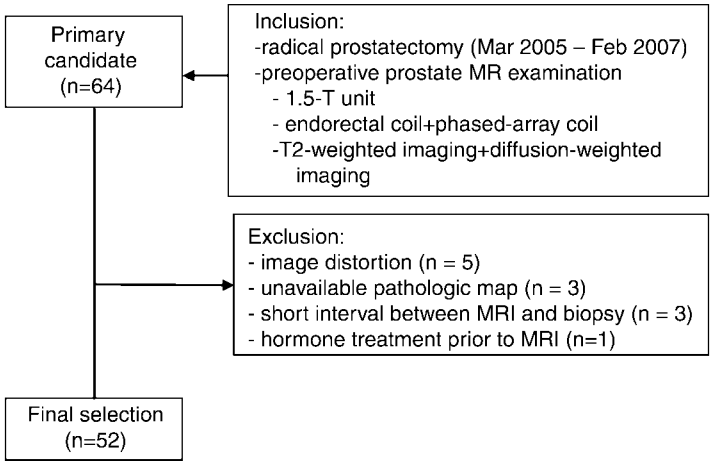

Figure 1: Flow diagram of patient selection.

criterion was the appearance of an area of homogeneously low signal intensity with ill-defined margins on T2-weighted images and ADC maps (14). Areas of low signal intensity on T2-weighted images and high signal intensity on T1-weighted images were considered indicative of hemorrhage after biopsy rather than cancerous tissue (15). According to these criteria, the probability for the presence of cancer in each segment was estimated by using a five-point rating scale: 1 indicated normal tissue; 2, probably normal tissue; 3, possible cancer; 4, probable cancer; and 5, definite cancer.

Statistical Analysis

To evaluate the diagnostic performance of the three MR imaging data sets for the detection of prostate cancer, receiver operating characteristic (ROC) analysis was performed. The areas under the ROC curves (AUCs) were then compared for each of the three data sets by each reader and between the readers for each data set by using the *Z* test. ROC study was performed by using software (MedCalc for Windows, version 7.4.1.0; MedCalc, Mariakerke, Belgium).

From the ROC curves, the optimal cutoff point was extracted, which showed the best separation (minimal false-negative and false-positive results) for prostate cancer detection. Sensitivity, specificity, and overall accuracy, which corresponded to the cutoff values, were then calculated and compared between data sets and between readers by using the *Z* test after adjusting for the effect of clustering according to literature references (16). Calculation of statistical parameters for the adjustment for data clustering and comparison of sensitivity, specificity, and accuracy was performed by using software (Excel for Windows, version 2003; Microsoft, Redmond, Wash).

In every statistical analysis, a *P* value of less than .05 was considered to indicate a significant difference.

Results

According to pathologic findings, there was prostate cancer in 227 (36%) of 624 segments and no cancer tissue in 397 (64%) of 624 segments. Prostate cancer was noted in 97 (31%) of 312 segments in the transition zone and in 130 (42%) of 312 segments in the peripheral zone. The mean number of segments with prostate cancer was 4.4 ± 2.2 (range, 1–12).

The AUCs of the three readers are shown in Table 1 and Figure 2, and a representative case is demonstrated in Figure 3. Sensitivity, specificity, and accuracy for cancer detection and the significant difference of these parameters between T2-weighted images alone and T2-weighted images and ADC maps together are shown in Table 2.

According to the ROC curves, a score of 4 was determined to be the cutoff value for determining the presence of prostate cancer in each segment. Consequently, segments with a

Table 1

AUCs for Prostate Cancer Detection for Three Readers

Reader	T2-weighted Images	ADC Map	T2-weighted Images and ADC Map	*P* Value*
1	0.79 (0.75, 0.82)	0.86 (0.83, 0.89)	0.90 (0.87, 0.92)	<.0001
2	0.75 (0.72, 0.79)	0.81 (0.77, 0.84)	0.88 (0.85, 0.91)	<.0001
3	0.66 (0.63, 0.70)	0.74 (0.70, 0.77)	0.76 (0.73, 0.80)	<.0001

Note.—Data in parentheses are 95% confidence intervals.

* Indicates difference between T2-weighted images and ADC map and T2-weighted images alone.

Figure 2

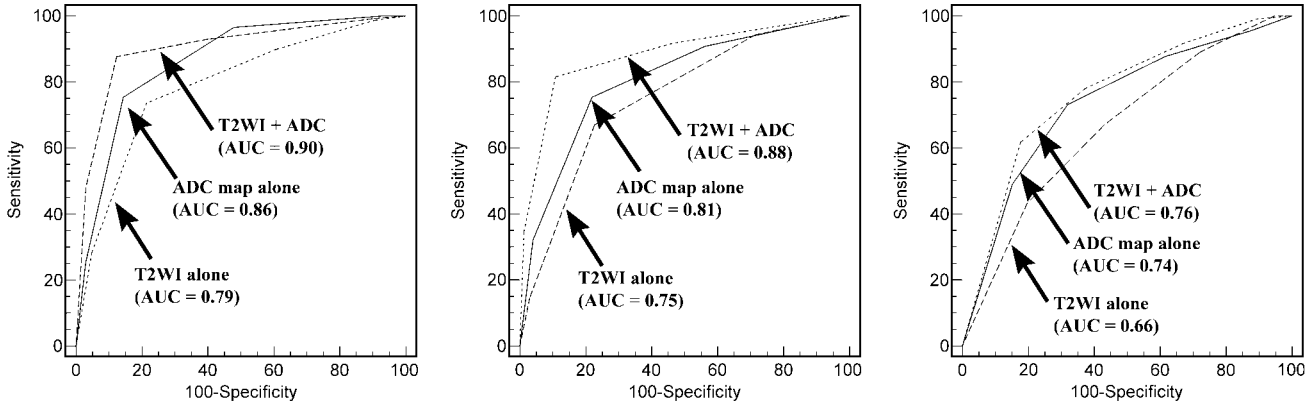

Figure 2: Graphs of ROC curves for prostate cancer detection for **(a)** reader 1, **(b)** reader 2, and **(c)** reader 3. *T2WI* = T2-weighted images.

Figure 3

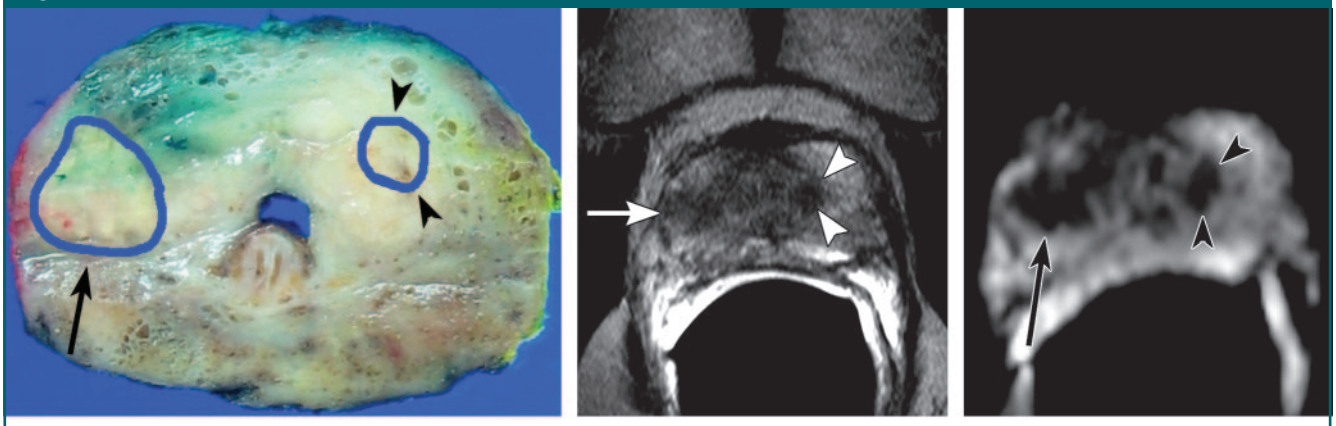

Figure 3: Imaging data in 68-year-old man with prostate cancer. **(a)** Histologic step section shows two outlined cancer areas in peripheral zone of right lobe (arrow) and transitional zone of left lobe (arrowheads). **(b)** Transverse T2-weighted MR image and **(c)** ADC map at the same level as **a**. Two lesions with low signal intensity in peripheral zone of right lobe (arrow) and in transitional zone of left lobe (arrowheads) are noted and are considered prostate cancer. On T2-weighted image, readers 1, 2, and 3 detected cancer only in the right lobe. On T2-weighted image and ADC map, readers 1 and 2 detected two cancer areas, while reader 3 detected a cancer area in the right lobe.

score of 4 or 5 were considered to have prostate cancer.

Comparison of Accuracy of Imaging Acquisitions

All three readers had greater AUCs for T2-weighted images and ADC maps than for T2-weighted images alone (reader 1, 0.90 vs 0.79; reader 2, 0.88 vs 0.75; reader 3, 0.76 vs 0.66) ($P <$ .0001 for all comparisons). For readers 1 and 2, the AUCs for T2-weighted images and ADC maps were greater than those for the ADC map alone (0.86 for reader 1 and 0.81 for reader 2) ($P =$ .036 for reader 1 and $P <$ .001 for reader 2).

All readers had greater sensitivity for T2-weighted images and ADC maps than for T2-weighted images alone (reader 1, 88% vs 74% [$P =$ .01]; reader 2, 81% vs 67% [$P =$ .02]; reader 3, 78% versus 67% [$P =$ .02]). For readers 1 and 2, specificity for T2-weighted images and ADC maps (88% and 89%, respectively) was greater than that for T2-weighted images alone (79% and 77%, respectively) ($P =$ .03 and $P <$ .001, respectively). All readers had greater accuracy for T2-weighted images and ADC maps than for T2-weighted images alone (reader 1, 88% vs 77% [$P <$ .001]; reader 2, 86% vs 77% [$P <$ .001]; reader 3, 68% versus 61% [$P =$ .04]).

Table 2

Comparison of Three Data Sets for Prostate Cancer Detection on a 12-Segment Basis for Three Readers

Parameter	T2-weighted Images	ADC Map	T2-weighted Images and ADC Map	*P* Value*
Reader 1				
Sensitivity	74 (167/227) [68, 79]	75 (171/227) [69, 82]	88 (199/227) [83, 93]	.01
Specificity	79 (312/397) [75, 83]	86 (340/397) [82, 89]	88 (348/397) [84, 91]	.03
Accuracy	77 (479/624) [73, 80]	82 (511/624) [79, 85]	88 (547/624) [85, 90]	<.001
Reader 2				
Sensitivity	67 (152/227) [60, 74]	75 (171/227) [68, 82]	81 (185/227) [76, 87]	.02
Specificity	77 (307/397) [73, 81]	78 (310/397) [74, 82]	89 (354/397) [86, 92]	<.001
Accuracy	77 (479/624) [73, 80]	77 (481/624) [74, 80]	86 (539/624) [84, 89]	<.001
Reader 3				
Sensitivity	67 (152/227) [60, 74]	74 (168/227) [66, 80]	78 (177/227) [71, 85]	.02
Specificity	57 (226/397) [52, 62]	68 (270/397) [63, 73]	63 (249/397) [58, 68]	.07
Accuracy	61 (378/624) [57, 64)	70 (436/624) [66, 73]	68 (426/624) [65, 72]	.04

Note.—Data are percentages, with numbers used to calculate percentages in parentheses and 95% confidence intervals in brackets.

* Indicates difference between T2-weighted images and ADC map and T2-weighted images alone.

Comparison of Reader Accuracy for T2-weighted Images and ADC Maps

With T2-weighted images and ADC maps, reader 1 had greater AUC (0.90 vs 0.76), sensitivity (88% vs 78%), specificity (88% vs 63%), and accuracy (88% vs 68%) than reader 3 ($P <$ .001 for AUC, specificity, and accuracy; $P =$ .04 for sensitivity). AUC, specificity, and accuracy were greater for reader 2 (0.88, 89%, and 86%, respectively) than for reader 3 ($P <$ .001 for all comparisons).

Discussion

In our lesion-based analysis, three readers with varying experience levels all showed greater AUC, sensitivity, and accuracy for prostate cancer detection with T2-weighted images and ADC maps than with T2-weighted images alone. Furthermore, for readers 1 and 2, specificity for prostate cancer detection was greater with T2-weighted images and ADC maps than with T2-weighted images alone. Therefore, our study suggests that the addition of an ADC map to T2-weighted images can significantly improve the diagnostic performance of MR imaging in prostate cancer detection.

Recent studies (17–19) have also shown the superiority of T2-weighted imaging and ADC to T2-weighted imaging alone in their lesion-based analysis. Results of the study by Haider et al (17) are comparable to ours, because they also obtained endorectal MR images with a 1.5-T unit. In their study, in which one experienced reader interpreted T2-weighted images alone and T2-weighted images and ADC maps together, the resulting AUC (0.87), sensitivity (81%), and specificity (84%) of T2-weighted images and the ADC map for prostate cancer detection were similar to those of our experienced radiologist (reader 1) (AUC, 0.90; sensitivity, 88% [199 of 227]; specificity, 88% [348 of 397]).

In addition to showing the incremental value of an ADC map for prostate cancer detection, our study also shows that the accuracy of the interpretation of T2-weighted images and ADC maps depends to some degree on the level of the reader's experience, as the AUC, specificity, and overall accuracy were greater for readers with a high or intermediate level of experience than for a less experienced reader. Moreover, with regard to the ADC map alone, AUC, specificity, and overall accuracy were greater for readers with a high or intermediate level of experience than for a less experienced reader. We suggest that this experience-dependent performance of interpreting T2-weighted images and ADC maps and the ADC map alone may be related to the qualitative process in the interpretation of the gray-scale ADC map. On a gray-scale display, only qualitative analysis based on the difference of ADC between voxels is apparent, but the actual value of the ADC is not displayed. Therefore, the interpretation of the ADC map is somewhat subjective for each reader, thus resulting in interobserver variability. To achieve more reliable results with the ADC map, it may be helpful to develop an advanced quantitative display method, such as the threshold-based color-display of ADC.

It is unclear how specific the ADC is for prostate cancer. The ADC is basically a parameter that displays the characteristics of the structural and magnetic environment that influences proton diffusion (20). The ADC then reflects various physical and physiologic characteristics of tissue but is not specific for cancer itself. Therefore, various abnormal conditions such as inflammation, ischemia, or benign prostatic hyperplasia, which cause structural changes, can alter the ADC value in a region of tissue (21). This nonspecificity of ADC for cancer tissue may result in an overlap of ADC between cancer and noncancerous tissue. Therefore, we suggest that the ADC map is helpful as a supplement to T2-weighted images rather than as a substitute for T2-weighted images.

A potential limitation of the ADC in cancer detection is its variability, as the diffusivity of a certain tissue may change according to biologic factors, such as a patient's age and body temperature, and technical factors, such as *b* value and location and area of region of interest (22–27). Therefore, the ADC threshold for the differentiation of cancer from noncancerous tissue may also vary, which makes it difficult to generally apply a certain ADC threshold for cancer detection. To overcome this potential limitation, normalized ADC, which is called relative ADC, can be calculated with ADC_{les}/ADC_{rs}, where ADC_{les} is the ADC of the lesion and ADC_{rs} is the ADC of the reference site. Normalized ADC seems to be necessary because normalization can reduce the variability of ADC caused by various patient or technical factors. The relative ADC is commonly used for brain imaging, which uses the contralateral brain area as reference tissue for calculating the relative ADC. We suggest that future efforts should therefore be made to determine the optimal relative ADC to be used for prostate cancer detection.

Diffusion-weighted imaging may be also potentially limited by organ motion, despite correct localization of the endorectal coil and inhibition of bowel peristalsis by the injection of hyoscine butylbromide, because organ motion may reduce the reliability of ADC map.

There were limitations to our study. First, because our study was a retrospective study, there may have been selection and verification biases. Moreover, because readers interpreted the MR imaging data with the knowledge that the patients had prostate cancer, there was a potential bias in that readers might have considered equivocal lesions as prostate cancer, thereby increasing the sensitivity.

Second, our study may be potentially limited by recall bias of the presence or absence of prostate cancer in a certain segment of the prostate. The review of an earlier MR interpretation session may have influenced the following MR interpretation. To minimize this bias, our image interpretation sessions were performed with a time interval of 4 weeks, and the three imaging data sets were evaluated in random order in each session.

Third, because our study included patients who underwent radical prostatectomy, there may have been a selection bias in that only patients with less aggressive and more localized prostate cancer were involved.

Finally, the correlation between imaging and histologic examination on a section-by-section basis has inherent limitations because the angle of the histologic slices may differ from that at MR imaging and the prostate usually shrinks during fixation. To reduce this potential limitation, we divided the prostate into 12 segments. Thus, the determination of the presence of prostate cancer in a segment was less affected by potential mismatching be-

tween MR imaging sections and histologic slices.

In conclusion, our study indicates that the addition of ADC maps to T2-weighted images provides significantly more accurate results than T2-weighted images alone for prostate cancer detection. Our results suggest that both the detection and localization of prostate cancer will improve if this technique is included in the routine MR imaging protocol.

Acknowledgment: The authors thank Gyunggoo Cho, PhD, Bio-MR Center, Korea Basic Science Institute, Chungcheongbuk-do, South Korea, for consulting on establishment of MR imaging acquisition protocol and manuscript editing.

References

1. Choi YJ, Kim JK, Kim N, Kim KW, Choi EK, Cho KS. Functional MR imaging of prostate cancer. RadioGraphics 2007;27:63–75.
2. Quint LE, Van Erp JS, Bland PH, et al. Carcinoma of the prostate: MR images obtained with body coils do not accurately reflect tumor volume. AJR Am J Roentgenol 1991; 156:511–516.
3. Hricak H, Choyke PL, Eberhardt SC, Leibel SA, Scardino PT. Imaging prostate cancer: a multidisciplinary perspective. Radiology 2007;243: 28–53.
4. Shimofusa R, Fujimoto H, Akamata H, et al. Diffusion-weighted imaging of prostate cancer. J Comput Assist Tomogr 2005;29:149–153.
5. Ichikawa T, Haradome H, Hachiya J, Nitatori T, Araki T. Diffusion-weighted MR imaging with a single-shot echoplanar sequence: detection and characterization of focal hepatic lesions. AJR Am J Roentgenol 1998;170:397–402.
6. Hosseinzadeh K, Schwarz SD. Endorectal diffusion-weighted imaging in prostate cancer to differentiate malignant and benign peripheral zone tissue. J Magn Reson Imaging 2004;20:654–661.
7. Tanimoto A, Nakashima J, Kohno H, Shinmoto H, Kuribayashi S. Prostate cancer screening: the clinical value of diffusion-weighted imaging and dynamic MR imaging in combination with T2-weighted imaging. J Magn Reson Imaging 2007; 25:146–152.
8. Reinsberg SA, Payne GS, Riches SF, et al. Combined use of diffusion-weighted MRI and 1H MR spectroscopy to increase accuracy in prostate cancer detection. AJR Am J Roentgenol 2007;188:91–98.
9. Pickles MD, Gibbs P, Sreenivas M, Turnbull LW. Diffusion-weighted imaging of normal and malignant prostate tissue at 3.0T. J Magn Reson Imaging 2006;23:130–134.
10. Miao H, Fukatsu H, Ishigaki T. Prostate cancer detection with 3-T MRI: comparison of diffusion-weighted and T2-weighted imaging. Eur J Radiol 2007;61:297–302.
11. Sato C, Naganawa S, Nakamura T, et al. Differentiation of noncancerous tissue and cancer lesions by apparent diffusion coefficient values in transition and peripheral zones of the prostate. J Magn Reson Imaging 2005;21:258–262.
12. Kim JK, Hong SS, Choi YJ, et al. Wash-in rate on the basis of dynamic contrast-enhanced MRI: usefulness for prostate cancer detection and localization. J Magn Reson Imaging 2005;22:639–646.
13. Zakian KL, Sircar K, Hricak H, et al. Correlation of proton MR spectroscopic imaging with Gleason score based on step-section pathologic analysis after radical prostatectomy. Radiology 2005;234:804–814.
14. Akin O, Sala E, Moskowitz CS, et al. Transition zone prostate cancers: features, detection, localization, and staging at endorectal MR imaging. Radiology 2006;239:784–792.
15. White S, Hricak H, Forstner R, et al. Prostate cancer: effect of postbiopsy hemorrhage on interpretation of MR images. Radiology 1995;195:385–390.
16. Zhou X, Obuchowski N, McClish D. Comparing the accuracy of two diagnostic tests. In: Statistical methods in diagnostic medicine. New York, NY: Wiley, 2002; 171–176.
17. Haider MA, van der Kwast TH, Tanguay J, et al. Combined T2-weighted and diffusion-weighted MRI for localization of prostate cancer. AJR Am J Roentgenol 2007;189: 323–328.
18. Kim CK, Park BK, Lee HM, Kwon GY. Value of diffusion-weighted imaging for the prediction of prostate cancer location at 3T using a phased-array coil: preliminary results. Invest Radiol 2007;42:842–847.
19. Yoshimitsu K, Kiyoshima K, Irie H, et al. Usefulness of apparent diffusion coefficient map in diagnosing prostate carcinoma: correlation with stepwise histopathology. J Magn Reson Imaging 2008;27:132–139.
20. Luypaert R, Boujraf S, Sourbron S, Osteaux M. Diffusion and perfusion MRI: basic physics. Eur J Radiol 2001;38:19–27.
21. Desouza NM, Reinsberg SA, Scurr ED, Brewster JM, Payne GS. Magnetic resonance imaging in prostate cancer: the value of apparent diffusion coefficients for identifying malignant nodules. Br J Radiol 2007;80: 90–95.
22. Hoehn-Berlage M, Eis M, Schmitz B. Regional and directional anisotropy of apparent diffusion coefficient in rat brain. NMR Biomed 1999;12:45–50.
23. DeLano MC, Cooper TG, Siebert JE, Potchen MJ, Kuppusamy K. High-b-value diffusion-weighted MR imaging of adult brain: image contrast and apparent diffusion coefficient map features. AJNR Am J Neuroradiol 2000;21:1830–1836.
24. Mulkern RV, Barnes AS, Haker SJ, et al. Biexponential characterization of prostate tissue water diffusion decay curves over an extended b-factor range. Magn Reson Imaging 2006;24:563–568.
25. Thoeny HC, De Keyzer F, Oyen RH, Peeters RR. Diffusion-weighted MR imaging of kidneys in healthy volunteers and patients with parenchymal diseases: initial experience. Radiology 2005;235:911–917.
26. Bilgili Y, Unal B. Effect of region of interest on interobserver variance in apparent diffusion coefficient measures. AJNR Am J Neuroradiol 2004;25:108–111.
27. Ulug AM, Beauchamp N Jr, Bryan RN, van Zijl PC. Absolute quantitation of diffusion constants in human stroke. Stroke 1997;28:483–490.